International Journal of Physics and Mathematical Sciences ISSN: 2277-2111 (Online)
An Online International Journal Available at http://www.cibtech.org/jpms.htm
2013 Vol. 3 (4) October-December, pp.132-143/Rajkumar and Alagar

Research Article

ANALOGY ESTIMATION OF CURRENT DENSITY, OHMIC POTENTIAL LOSS IN THE COPPER ELECTROLYSIS CELL MODEL

***S. R. Rajkumar[1] and M. Alagar[2]**
[1]*Department of Physics, Rajapalayam Rajus' College, Madurai Kamaraj University, Rajapalayam-626117, Tamil Nadu, India*
[2]*Department of Physics, Ayya Nadar Janaki Ammal College (Autonomous), Madurai Kamaraj University, Sivakasi -626124, Tamil Nadu, India*
**Author for Correspondence*

ABSTRACT

A computational model of a Copper electrolysis cell is presented. The model includes the microscopic mass transfer, electric field effects and the effects of the ohmic loss of potential in the cell bulk electrolyte. Estimation for the cell ohmic loss is created by utilizing electric field model of the cell and the function is applied to include the effects of ohmic loss to the cell model. The model structure enables computing the cell current, the electrode overpotential and the cell ohmic loss, with the only model input variable being the cell voltage. The cell model is implemented as a coupled computational model, which is solved with the finite elements method. In an electrolysis cell, whose dimensions can be accurately adjusted and measured. The electrode equation parameters are found by fitting the model against the data of one experiment, after which the model is evaluated against three other measurements.

***Keywords**: Current Density Cell Modeling, Copper Electrolysis, Electrode Equation, Computational Electrolysis, Ohmic Loss.*

INTRODUCTION

The important industrial application of copper electrodeposition is the manufacturing process of Printed Circuit Boards (PCBs). In modern PCBs, the circuit is created on several board layers, and interconnections between these layers are also made within the board, in the copper electroplating process known as micro by way of filling (Moffat *et al.,* 2000).This work depicts copper electrolysis cell model for the electrode processes, as well as the cell geometry and the corresponding ohmic loss of potential in the bulk electrolyte, in a single computational system, with a reasonable computational attempt. The presented model structure is trusted to make scaling up of computer models effortless, by slot in the effects that the physical dimensions of the cell apparatus have on the estimates produced by the model. Still more studies have been published related to similar processes that are applied in microchip production, where the time and length scales are ca. hundred-fold smaller (Kondo *et al.,* 2003; Vereecken, 2005; Newman and Thomas, 2004).

In a conventional micro by way of fill electroplating system, where the plated boards are positioned vertically between two soluble anodes, the distance between the anode and the cathode can be altered up to 30 cm. The Copper deposition process is typically controlled galvanostatical DC regulated power supply (Aplab L 3230), so that a cell current, that corresponds to a desired average cathode current density, is maintained in the cell by (automatically) adjusting the cell power source output. As a current flows through the cell, the distance between the electrodes and the resistance of the electrolyte cause an ohmic drop of electric potential (*iR* -drop) to occur over the electrolyte (Newman and Thomas, 2004) were recorded for every 30 seconds up to 30 minutes . Even though a supporting electrolyte is regularly used in industrial PCB production lines, the ohmic loss over the electrolyte is still notable due to the distance between the electrodes (Khandpur, 2005). In order to maintain a desired average plating current density, the cell power source must compensate for the iR -drop by increasing the potential difference between the electrodes. As a result, the electrode potentials are directly affected by the ohmic loss in the bulk electrolyte.

No reference electrode is typically available by way of fill electroplating system, because such a device would become unreliable due to contamination. The cathode potential cannot be directly measured. Recent studies show that the electrolyte additives affect the copper reduction reaction, is dependent on the cathode potential (Li *et al.,* 2009; Moffat *et al.,* 2005). Also, the electrode potentials are important factors for the cell current efficiency (Pletcher and Walsh, 1990) and be considered when high-performance cells are designed. Several computational models in both the sub-micron scale and the micrometer scale have also been accounted (Andricacos *et al.,* 1998; West *et al.,* 2001; Georgiadou *et al.,* 2001; Moffat *et al.,* 2007).

Usually the presented models in spatial dimensions that is equal to those of the modeled surface feature. It is also the phenomena taking place in the bulk of the physical system affect the fill process. The phenomena included in the system model distance a wide range in magnitude, in both scales of time and length, which presents a multiscale modeling problem. This problems call for an opinion of the computational implementation techniques for including the individual sub-processes to the model. The presented model produces estimates for all of the mentioned sub-processes, i.e., the current densities and (over) potentials on the electrodes, as well as the ohmic potential drop over the electrolyte. The model is structured so that it enables incorporating the sub-models, which describe the microscopic phenomena taking place within micrometers (or nanometers) from the electrode surface, and those describing the electric potential loss phenomenon in the bulk electrolyte, into the same computational system.

MATERIALS AND METHODS

The experimental apparatus

The reported model structure is illustrated in Figure 1 and 1.1. The distance (L) between the counter electrode (CE) and the working electrode (WE), and the electrolyte depth (D) can be adjusted, but the width of the cell is constant (5 cm). The working electrode is connected to the positive point of the DC power source, which is relevant to signs of potential variables are considered. The cell design is simple, so that the cell was constructed; the dimensions of the cell and of the electrodes can be accurately adjusted and measured the effects that the physical dimensions of the cell have on the cell current–voltage response. It is illustrated how the cell dimensions are included in the cell model as input parameters, and how a three-dimensional electric field model of the experiment cell is utilized to determine a function for estimating the ohmic loss over the cell bulk electrolyte.

The current density related to the rate of an electrochemical reaction at a single electrode–electrolyte interface as a function of the electrode over potential (Pohjoranta and Tenno, 2007). Ohm’s law yields the potential difference over a non-ideal conductor, carrying a known current. By considering the electrolysis cell as a system consisting of two electrode–electrolyte interfaces that are connected by a non-ideal conductor (the electrolyte), the cell can be divided into three sub-systems, which are all coupled. The coupling between the subsystems is formed by the cell current and the cell voltage, which both are easily measurable. Also the implemented cell model contains three coupled sub-models, which are solved simultaneously. Firstly, the electrochemical reactions, as well as the microscopic mass transfer phenomena and the electric field close to both of the two electrodes are modeled. This produces a partial differential equation (PDE) system, which is solved with a finite elements method (FEM). Secondly, the effects of the iR -drop over the bulk electrolyte are included to the FEM model i.e., with a function. However, because the electrode current density is a non-linear function of cell voltage as function is utilized.

A systematic description of the function and its evaluation is found in (Corless *et al.,* 1996), and some examples of its application in physics have been documented (Valuri *et al.,* 2000).The function has previously been utilized to obtain semi analytical and numerical solutions for problems related to transistors and diodes (Chen *et al.*, 2007; Banwell, 2000; Jung and Guzeiwicz, 2009; Jain *et al.*, 2006), and also to solar cells (Ding and Radhakrishnan, 2008; Kelly *et al.*, 2003; Bard and Faulkner, 2001). The common characteristics of the cell model are the descriptive equations contain the exponential function. As the function is utilized to couple the electrode subsystems to the ohmic loss over the bulk electrolyte, estimating the processes on the electrodes with potential.

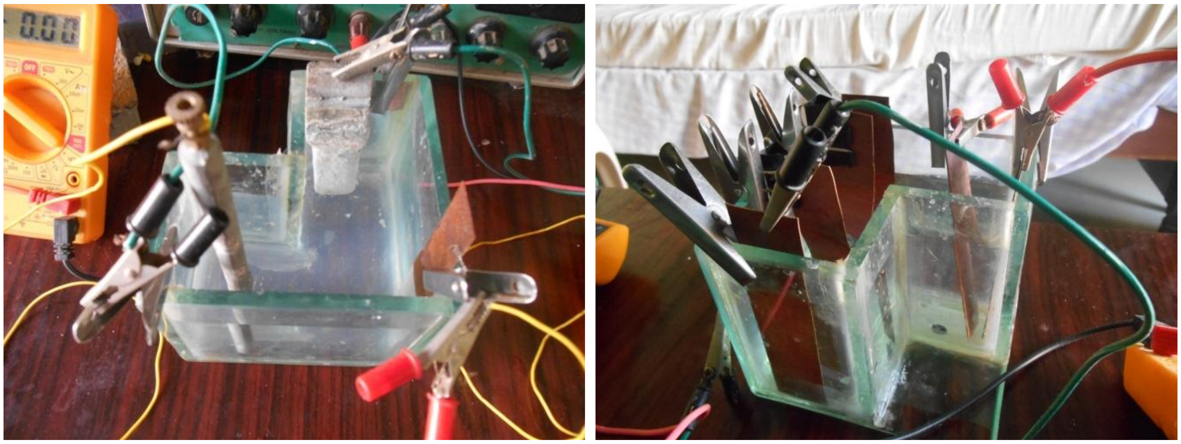

Figure1: Photo graphs of the cell model structure:

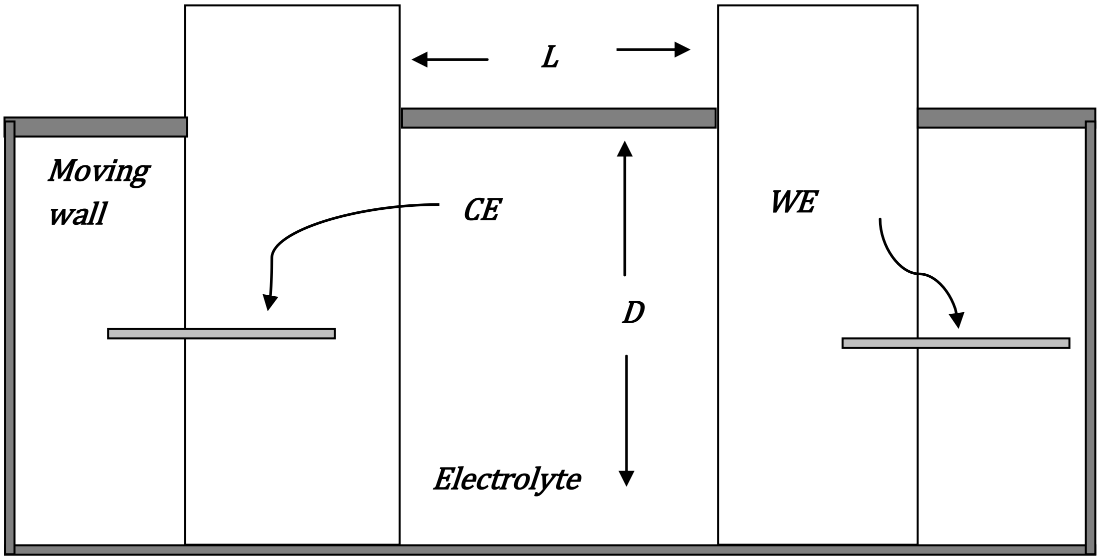

Figure 1.1: Schematic view of the cell .D -is electrolyte depth, L -is cell length, CE and WE -counter electrode and working electrode surface.

Though, as mentioned, the industrial copper plating processes are galvanostatic controlled experiments were chosen for model development. The model parameters are determined based on one reference case then the model is evaluated, where the cell dimensions are modified. To keep only an aqueous $CuSO_4$ electrolyte is used in the experiments. It should be noted, however, that in practical copper electroplating baths, a supporting electrolyte is normally used.

The cell iR-drop estimate U_{Ω}

The primary potential distribution (Newman and Thomas, 2004; Haung and Hibbert, 1995) inside the cell is examined. The potential distribution in the cell is solved by assuming a homogenous electrolyte domain, with a constant electric conductivity b (S m−1). For this study, the assumption is justified by the short duration of the plating experiments described in the following Section and the small ratio of the electrode areas versus the electrolyte volume in the apparatus (Newman, 1966). It is considered that the solution concentration in the bulk remains approximately constant and homogenous throughout the experiments. In practical plating system the bulk electrolyte would be continuously agitated and, therefore, no concentration gradients would exist. The 3D model geometry is configured to match that of the experiment cell (Figure 1 and 1.1) with varied length (L) and varied cross-sectional area (W× D). The potential field inside the cell is then solved with the Poisson equation

$$\nabla.(-\sigma\nabla\phi) = 0 \qquad [1]$$

Where ϕ is the electric potential (V) and σ is the electric conductivity(S/m) of the electrolyte. $\sigma -$ is given the value that is measured for the electrolyte conductivity as described in Section 5 and, therefore, $\sigma = \sigma_b$ = b= 3.35 S/m. The boundary condition $\phi = 0$ set on one electrode boundary and a constant, but varied, average current density i_{set} (A/m^2) is set on the other electrode boundary

$$-n.(\sigma\nabla\phi) = i_{set} \qquad [2]$$

The current density boundary condition (equation 2) should be considered an average condition because a current density is set; the current density on the boundary is not constant over the complete boundary. In addition, with the given boundary condition, the integral of the current density over the electrode, divided with the electrode area equals the set current density. The purpose of the described static electric field model is only to clarify the primary potential distribution inside the cell when the cell dimensions change, so that an estimate for the cell iR –drop can be formulated. The actual electrochemical system is not included in this model and only the primary potential distribution, obtained by solving (equation 1) in a perfectly homogenous electrolyte domain, is examined. Though the primary potential distribution model is only an approximation of the electric field in the electrochemical system, this approach was chosen to keep the analysis simple. The main aim with the model noted here to find a lumped estimate for U_{Ω} which is linear with respect to cell current.

Electric field simulation results

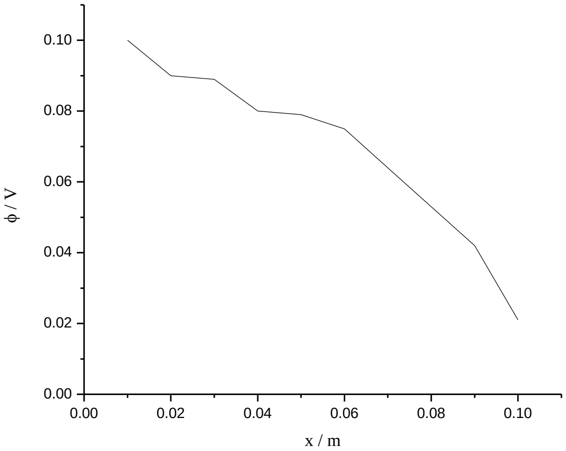

Figure 2: The electric potential ϕ along a straight line connecting the center points of the electrodes. Boundary conditions are given as a zero-potential on one electrode and a current density of 200 A/m^{2}on the other electrode

The results of the electric field simulation are in line with the well known analytical results (Mandin *et al.,* 2004; Takahashi and Gross, 1999). In the bulk of the domain the potential changes linearly in the direction of the cell length, and close to the electrodes the potential changes non-linearly. Figure 2 illustrates the electric potential level ϕ on a straight line from the center point of the anode to the center point of the cathode, when the modeled cell length L = 10 cm (D = 1.5cm, W = 1.0 cm).

The simulated potential field inside the cell in three different cases of cell length can be seen that when the electrodes are close to each other (L = 3 cm), the electric field is very irregular over the whole electrolyte. Conversely, when the electrodes are further apart, an area of a very regular electric field exists in the cell. A close-up of the electric equipotential levels near the electrode surface is l = 0.1 m. The potential equipotential very near the electrode surface form hemispherical planes, as described by Newman in (Newman, 1966) .As a conclusion of examining Figure2, along with the known analytical results, the cell ohmic loss is estimated with a function consisting of three distinct parts:

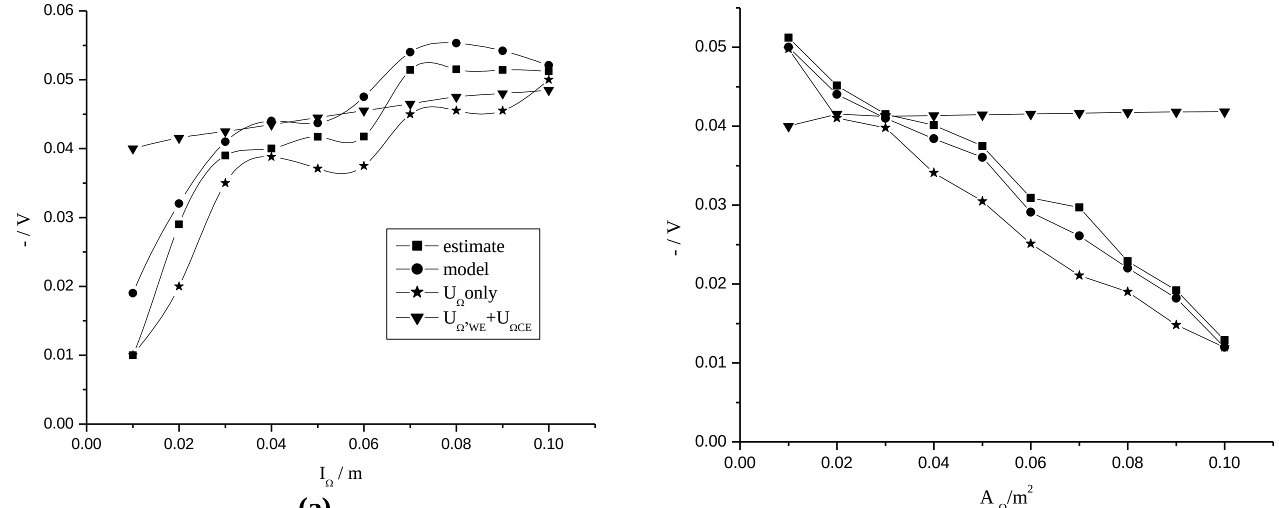

(a)

(b)

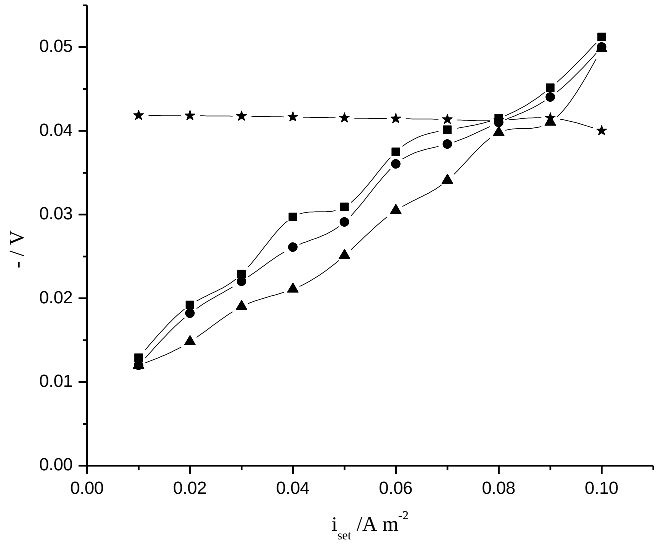

(c)

Figure 3: Effect of (a) the cell length (l_Ω), (b) the cell cross-sectional area (A_Ω= W× D) and (c) the set electrode current density (i_{set}) on the ohmic loss estimate. Also thevalues obtained by using $U_{\Omega,b}$ and$U_{\Omega,WE} + U_{\Omega,CE}$ are plotted to illustrate the effect of each term. In Figures (a) and (b), the boundary condition current density is set to 200 A/m^{2}and in Figure (c) the cell length is 0.1 m and cross-sectional area 8.5 × 10^{-4}m^2

The estimate for the main bulk, $U_{\Omega,b}$

In the main bulk electrolyte the ohmic loss is estimated by assuming both the electrolyte composition and the current density distribution homogenous (Equation 3). This corresponds to considering the bulk electrolyte as resistor material.

$$U_{\Omega,b} = R_{\Omega} I_{cell} = \frac{l_{\Omega}}{A_{\Omega}\sigma_b} i_{WE} A_{WE} \qquad [3]$$

In Equation 3: $l -$ is the mean length (m) and A_{Ω} −the mean cross-sectional area (m^2) of the current path in the electrolyte, which are here approximated with L and W X D , respectively.

The estimate near the electrodes, $U_{\Omega,e}$

The estimate for ohmic loss in the area close to the electrodes, where the electric field and the current density field are non-uniform, is based on the geometrical analysis given in (Newman, 1966). Because the electrodes are shaped, the electric equipotential levels are assumed to adopt the shape of oblate hemispheres near the electrodes. The (hypothetical) potential difference ΔU from an equipotential level at ξ in the electrolyte, to an electrode through which a total current $A_e i_e$ (A) passes, can be then formulated as a function of ξ as $\Delta U = r_e i_e/(2\sigma_b)\ \tan^{-1} \xi$. Here ξ is the first coordinate in the rotational elliptic coordinate system in[24]. r_e −is the radius of the electrode disk (m) and i_e − the average current density (A/m^2) on the electrode. At the limit, when ξ approaches infinity, the potential difference becomes $\pi r_e i_e/(4\sigma_b)$.

As is shown in (Newman, 1966), the potential difference between the electrode and ξ increases rapidly when the areas near the electrode is examined. This phenomenon is also seen in Figure 2, at both ends of the plot. Therefore, the limit value for ΔU is adopted here as the ohmic potential loss estimate at the electrodes and

$$U_{\Omega,e} = \frac{\pi r_e}{(4\sigma_b)} i_e \qquad [4]$$

Full cell ohmic loss estimate

The full ohmic loss estimate is a sum of the terms in the bulk and near both of the electrodes, and is a linear function ofi_{WE} , as given in (Equation 5) and (Equation 6).

$$U_{\Omega,e} = i_{WE} K_{\Omega} \qquad [5]$$

$$K_{\Omega} = \frac{\pi r_{WE}}{\sigma_b}\left(\frac{r_{WE}\, l_{\Omega}}{A_{\Omega}} + \frac{1}{4} - \frac{1}{4\sqrt{k_A}}\right) \qquad [6]$$

Comparison of the estimate and the model

The estimate for the cell ohmic loss (Equation 5) is compared against the estimate in Figure 3. For the estimate, the plotted value is the potential difference between the electrodes. The estimate does overestimate the cell ohmic loss slightly, presumably because the electrodes are not infinitely far apart, which was assumed when formulating (equation 4). In Figure 3 (a), the estimate error, calculated as the difference between the estimates, are from−3mV to −4 mV, when the cell length is above 3 cm. In Figure 3(b) the error is from 2 mV to−4 mV over the whole simulation range and in Figure3(c) the maximum error is −14 mV. Therefore, the estimates and the model can be observed to match rather well when the cell length is above 3 cm. For comparison, the estimate for ohmic loss in the main electrolyte bulk only,$U_{\Omega,b}$ as well as the sum of the estimates near the electrodes, $U_{\Omega,WE} + U_{\Omega,CE}$ are also shown. It is clear that neither of these alone would be a satisfactory estimate. The estimate can be observed to correspond sufficiently well with the model when the cell length is above 3 cm.

It is presumed, that when the estimate obtained by using the model is utilized in the electrolysis cell model, the quality of the final modeling results also express the quality of the estimate and model, equally.

The electrolyte domain

Mass transfer

Mass balance of the $Cu^{2+}$and SO_4^{2-}ions are considered in the model. The copper redox reactions cause a concentration gradient in the electrolyte close to the electrode surfaces and, consequently, mass transfer of these ions arises. Mass transfer is considered to be dominated by diffusion and migration (Newman and Thomas, 2004), with the electroneutrality condition valid, i.e., $\sum z_i c_i=0$, where $c_i -$ is the concentration (mol/m^3) of species i.

$$\frac{\partial c_i}{\partial t} = \nabla . (D_i \nabla c_i + z_i \frac{D_i}{RT} F c_i \nabla \phi) \qquad [7]$$

Convective mass transfer is not considered because (i) no agitation of the electrolyte is applied in the experiments and (ii) natural convection caused by density variations in the electrolyte are assumed small due to the short duration of the plating experiments. Several studies related to the mass transfer effects of convection have been published, e.g. (Mandin *et al.*, 2004; Takahashi and Gross, 1999; Dow *et al.*, 2005; COSMOL, 2008; Coombs, 2008; Kanagasabapathy) and, clearly, convective mass transfer should be considered separately per case.

The initial distribution of species is assumed uniform all over the system and equal to the bulk solution conditions, i.e.

$$-n. \left(D_{cu} \nabla c_{cu} - F z_{cu} \frac{D_{cu}}{RT} c_{cu} \nabla \phi \right) = n_{a,e} \qquad [8]$$

$n -$ denotes the boundary outward normal vector.

The electric field

The electric potential $\phi(V)$ is solved based on the conservation of charge and coupled to the Nernst–Planck mass transfer system(12) .Conservation of charge is maintained by setting $\nabla . \mathbf{i} = 0$, where $\mathbf{i} = F \sum z_i \left(D_i \nabla c_i + F z_i \frac{D_i}{RT} c_i \nabla \phi \right) = i_e$ is the current density (A/m^2)corresponding to the mass transfer of ions in the electrolyte.

The boundary conditions are given as a fixed potential condition on one electrode boundary, where $\phi = \Delta\phi_e$, and as a current density condition (Equation 9) on the other electrode boundary.

$$-n. F z_{cu} \left(-D_{cu} \nabla c_{cu} - F z_{cu} \frac{D_{cu}}{RT} c_{cu} \nabla \phi \right) = i_e \qquad [9]$$

In order to reduce the cell model size, mass transfer and the electric field in the bulk electrolyte are not included in the cell model explicitly.

Cell potential and cell current

The electromotive force driving the electrolysis is the cell power source output voltage, denotedE_{out} (V). E_{out} is consumed in the work done on the metal–electrolyte interfaces in order to transfer charge and mass according to (Equation 7), and in the bulk electrolyte to conduct current through it. The potential loss corresponding to the work done in the charge transfer reactions is represented by the electrode overpotential, denoted η_{WE} andη_{CE}. The cell ohmic loss beingU_Ω(V), the cell voltage can be written as a sum of these three components (Equation 11).

$$E_{out} = \eta_{WE} - \eta_{CE} + U_\Omega \qquad [10]$$

The contribution of concentration overpotential is not shown explicitly in (Equation 11). However, the potential of both electrodes is measured versus the same reference point; the concentration overpotential contribution is included through the electrode equilibrium potential terms in (Equation 11).

Cell current

The cell current, I_{cell}(A) can be computed based on the electrode area (A_e ,m^2) and electrode current density (i_e) of either one of the electrodes; $I_{cell} = A_e i_e$. Furthermore, since only one current runs through the cell, it couples the electrode current densities in proportion to their surface areas as

$$A_{WE} i_{WE} + A_{CE} i_{CE} = 0 \qquad [11]$$

Equation (11) is utilized to derive the expressions for the potential components η_i and U_Ω on the RHS of (Equation 10)

Overpotential terms

In the following, it is described how the working electrode over-potential (WE) is obtained as a function of the cell power source output E_{out}. The same applies to the equation for the WE current density (i_{WE}), which is also introduced below.

The coupling between WE and E_{out} is obtained through the Butler-Volmer Equation (8) and the Kirchhoff's laws applied on the cell circuit. The bi-directional form of Equation (8), however, does not enable solving electrode overpotential analytically and, therefore, a one-directional approximation of Equation (8) at each electrode is taken as the starting point. Equation (11) is applied next to couple the electrode current densities (i_{WE} and i_{CE}) together through the electrode areas, which enables eliminating i_{CE} from the equation system. Similarly, the voltage law Equation (10), enables formulating CE as function of WE, and thereby, enables eliminating CE from the equation system. The ohmic loss of potential occurring in the cell (U_Ω) is approximated with the estimate in Equation (5), which gives U_Ω as a function of the cell geometry, the bulk electrolyte conductivity and the working electrode current density.

Model implementation

All simulations were carried out using the Multiphysics solver software (Kanagasabapathy; MATLAB; Weisstein, 2008 Subramanian, 2006) and a desktop PC (2.4 GHz 2 Quad, 3.24 GB). The finite elements method (FEM) to solve the partial differential equation systems and standard, second order Lagrangian shape functions were used in all cases.

The Nernst–Planck mass transfer system for Cu^{2+} and SO_4^{2-} ions coupled with the electric field in the area of the electrodes was configured as an axially symmetric model. Though smaller than what would be allowed by the experiment apparatus, the model domain at each electrode was made wide enough so that no concentration change could be observed at the model boundaries during the simulations.

Table 1: Cell dimensions in the experiments.

Case	L × D × W(m × m × m)	A_{WE} (m^2)	A_{CE} (m^2)
S_1	0.03× 0.021 × 0.005	7.85×10^{-7}	1.65×10^{-6}
M	0.10× 0.017 × 0.005	7.85×10^{-7}	1.65×10^{-6}
L	0.16× 0.017 × 0.005	7.85×10^{-7}	1.65×10^{-6}
S_2	0.03× 0.028 × 0.005	7.85×10^{-7}	7.85×10^{-7}

Table 2: The geometric model parameters corresponding to the experiment cases (l_Ω = L , A_Ω= D × W, $k_A = A_{CE}/A_{WE}$).

Case	l_Ω	A_Ω (m^2)	k_A
S_1	0.03	1.05×10^{-4}	2.1
M	0.10	8.5×10^{-5}	2.1
L	0.16	8.5×10^{-5}	2.1
S_2	0.03	1.4×10^{-4}	1 .0

Experimental

The cell described in Figure 1. Aqueous $CuSO_4$in a concentration of 500 mol/m^3 was used as the electrolyte solution in all tests. The electrolyte was prepared by dissolving AR grade copper sulfate ($CuSO_4\cdot 5H_2O$) in deionized water. Cross-sectioned copper wires with a diameter of 1.0 cm X 1.5 cm, imbedded in counter electrodes. The electrodes were polished and rinsed with sulfuric acid and deionized water before each experiment series. The cell width (W) was constant at 0.5 cm in all tests, but the cell depth (D) was varied from 2.0 cm to 3.0 cm and the cell length (L)was varied from 3 cm to 15 cm, in order to modify the cell resistance between experiments.

In addition, the effect of the electrode area ratio (k_A) was tested by varying the counter electrode (CE) copper wire of electrolytic grade (99.6%) diameter from 1.0 x 1.5 cm^2. This corresponds to a variation from 1 to 2 in the electrode area ratio, which is in the range of typical PCB manufacturing line operating conditions (Moffat *et al.,* 2000). The working electrode (WE) diameter was constant at 1.0 x 2.0 cm^2 in all experiments.

In all experiments, the cell voltage was swept from 0V to−0.5 V and with a sweep rate of 50 mV/s, as also shown in Figure 4 (E_{out}). The working electrode overpotential was measured against reference electrode (RE) was saturated calomel electrode (SCE, E^o=+0.2422 V). All experiments were repeated and the results were found consistent.

RESULTS AND DISCUSSION

The electrolysis cell model geometry was configured according to the dimensions measured from the experiment cell Table 1. Electrode morphology was considered equal on both electrodes and, therefore, omitted from the model. The electrodes were assumed perfectly the geometric areas of the electrodes were used as the electrode areas. During model validation, the estimates produced by the model were compared to the data from the other experiment cases, while keeping all other but the geometric parameters in the model constant. The geometry parameters were changed according to the experiment conditions, as listed in Table 2. The simulation results are shown in Figs. 4–9. Figure 4 illustrates the electric potential components in the cell system as estimated by the model in the reference case S_1.

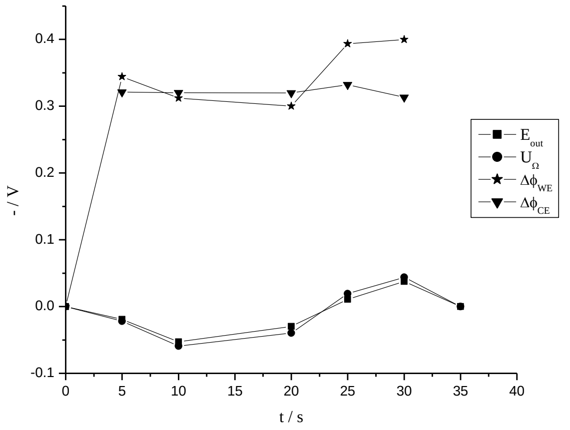

Figure (4)

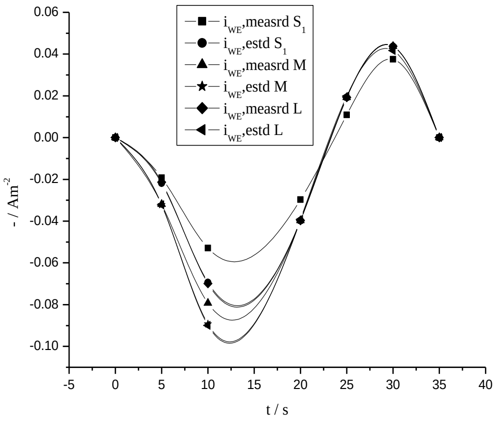

Figure (5)

Figure 4: Cell potential E_{out} , potentials U_Ω, $\Delta\phi_{WE}$ E ; $\Delta\phi_{CE}$ as estimated by the model.

Figure 5: WE current density- cases S_1, M and L. (cell length, *l*, changes 3 cm to 15 cm.)

The electrode potentials are calculated with Equation (10) and the electrolyte ohmic loss with Equation (5). Also the cell power source output (E_{out}) is given.

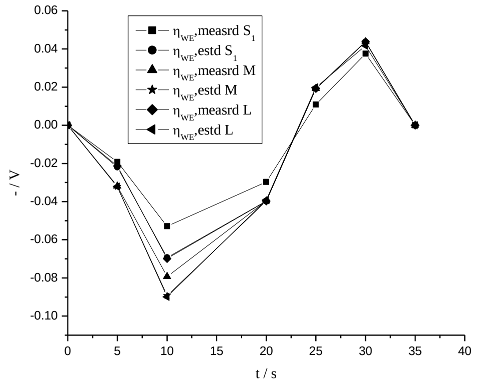

Figure (6)

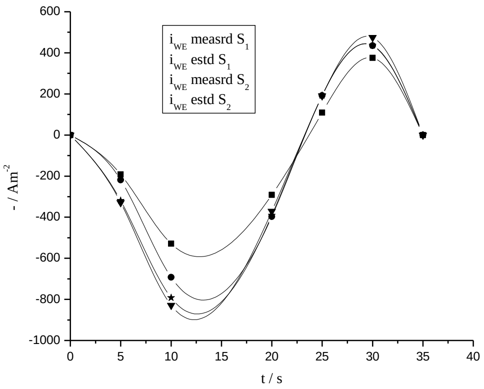

Figure (7)

Figure 6: WE overpotential - cases S_1, M and L.
Figure 7: WE current density - cases S_1 and S_2 . (Electrode area ratio, k_A, changes from2.1 to 1.)

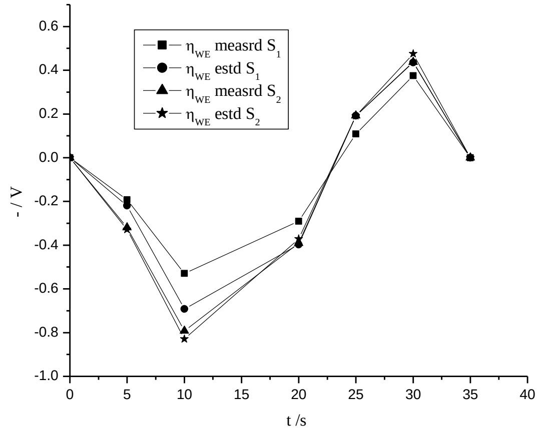

Figure (8)

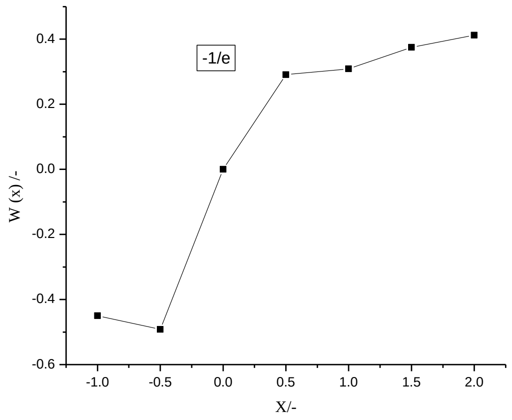

Figure (9)

Figure 8: WE overpotential -cases $S_1$and S_2.
Figure 9: Output of the numerical function close to −1/e.

Figs. 8 and 9 show the estimate for the WE current density (i_{WE}) and overpotential (WE), and the corresponding measured values, when the cell dimensions are varied. A small difference between the estimated and measured curve can be consistently observed during the return part of the cathodic sweep in both figures.

The proportional error is within ±3% of measured value during 0–10 sec of the sweep, but rises up to 30% close to the 30 sec time instant, when the current is small. In the compared cases, the error is similar but slightly smaller. Analogously to the current density estimate, also the reference case estimate for the WE overpotential (Figure 9) deviates from −5 mV to 20 mV from the measured value, depending on the sweep time instant.

A model structure that enables incorporating the ohmic loss of potential over the bulk electrolyte to an electrolysis cell model was presented. A lumped estimate for the cell ohmic potential loss was created by utilizing a 3D model of the primary potential distribution in the cell. It was found that the ohmic loss obtained with the examined 3D model can be fairly accurately estimated with a scalar function of the cell geometry, the bulk electrolyte conductivity and the cell current. The cell model was implemented computationally as a Finite Elements Model (FEM) including the estimate for ohmic loss. The model was found computationally light, feasible for online control development purposes. The electrode equation parameters for the cell model were found by fitting the model output with the data of one reference case measurement.

REFERENCES

Alan West C, Mayer S and Reid J (2001). A Super filling Model that Predicts Bump Formation. *Electrochemical* and *Solid State* Letters **4** (7) C50-C53.

Andricacos PC, Uzoh C, Dukovic JO, Horkans J and Deligianni H (1998). Damascene copper electroplating for chip interconnections. *IBM Journal of Research and Development* **42**(5) 567-574.

Banwell TC and Jayakumar A (2000). Exact analytical solution for current flow through diode with series resistance. *Electronics Letters* **36**(4) 291 – 292.

Bard A and Faulkner L (2001). *Electrochemical Methods; Fundamentals and Applications (*John Wiley and Sons Inc, New York) ISBN 0-4471-04372-9. 33.

Chen R, Zheng X, Deng W and Wu Z (2007). A physics-based analytical solution to the surface potential of polysilicon thin film transistors using the Lambert W function. *Solid-State Electronics* **51**(6) 975-981.

COMSOL AB (2008). COMSOL Multiphysics User Guide and Model Library, version 3.5a,3.5.0.606, Sweden. Available: http://www.comsol.co.in/products/tutorials-35a/

Coombs Clyde JF Jr. (2008). *Printed Circuits Handbook* 6th edition (eBook, McGraw-Hill, New York) ISBN 9780071467346.

Corless R, Gonnet G, Hare D, Jeffrey D and Knuth D (1996). On the Lambert W-function. *Advances in Computational Mathematics* **5**(1) 329- 359.

Ding J and Radhakrishnan R (2008). A new method to determine the optimum load of a real solar cell using the Lambert W-function. *Solar Energy Materials and Solar Cells C* **92** (12) 1566-1569.

Dow WP, Huang HS, Yen MY and Huang HC (2005). Influence of Convection-Dependent Adsorption of Additives on Micro via Filling by Copper Electroplating. *Journal of Electrochemical Society* **152**(6) C425-C434.

Georgiadou M, Veyret D, Sani RL and Alkire RC (2001). Simulation of Shape Evolution during Electrodeposition of Cop*per* in the Presence of Additive. *Journal of Electrochemical Society* **148**(1) C54-C58.

Huang W and Brynn Hibbert D (1995). Modeling of metal electrodeposits: Analytical solutions *Physical Review E* **52**(5) 5065-5069. Available: http://link.aps.org/ doi/10.1103/ PhysRevE.52.5065

Jain A, Sharma S and Kapoor A (2006). Solar cell array parameters using Lambert W-function. *Solar Energy Materials and Solar Cells C* **90**(1) 25–31.

Jung W and Guziewicz M (2009). Schottky diode parameters extraction using Lambert W function. *Materials Science and Engineering B* **165**(1-2) 57-59.

Kanagasabapathy M (No Date). Technical computation by MATLAB, Math Forum (Research), Drexel University Philadelphia, USA. Available: http://mathforum.org/ library/view/ 75575. html

Kelly R, Scully J, Shoesmith DW and Buchheit R (2003). *Electrochemical Techniques in Corrosion Science and Engineering* (Marcel-Dekker Inc. New York), ISBN: 0-8247-9917-8 18.

Khandpur R (2005). *Printed Circuit Boards: Design, Fabrication and Assembly* 2nd edition (eBook, McGraw-Hill Electronic Engineering) 691.

Kondo K, Yamakawa N, Tanaka Z and Hayashi K (2003). Copper damascene electrodeposition and additives. *Journal of Electroanalytical Chemistry* **559** 137-142.

Li YB, Wang W and Li YL (2009). Adsorption Behavior and Related Mechanism of Janus Green B during Copper Via-Filling Process. *Journal of Electrochemical Society* **156**(4) D119-D124.

Mandin Ph, Pauporté Th, Fanouillère Ph and Lincot D (2004). Modeling and numerical simulation of hydro dynamical processes in a confined rotating electrode configuration. *Journal of Electroanalytical Chemistry* **565**(2) 159-173.

MATLAB [No Year]. Technical computations by MATLAB. Available: http://techmatlab.blogspot.in.

Moffat T, Bonevich J, Huber W, Stanishevsky A, Kelly D, Stafford G and Josell D (2000). Superconformal Electrodeposition of Copper in 500–90 nm Features. *Journal of Electrochemical Society* **l47**(12) 4524-4535.

Moffat T, Wheeler D, Edelstein M and Josell D (2005). Super conformal film growth: Mechanism and quantification. *IBM Journal of Research and Development* **49**(1) 19-36

Moffat T, Wheeler D, Kim SK and Josell D (2007). Curvature enhanced adsorbate coverage mechanism for bottom-up super filling and bump control in damascene processing. *Electrochimica Acta* **53**(1) 145-154

Newman J (1996). Resistance for Flow of Current to a Disk. *Journal of Electrochemical Society* **113**(5) 501-502.

Newman J, Karen Thomas and Alyea E (2004). *Electrochemical Systems* 3rd edition (John Wiley andSons Inc. Publication, Hoboken, New Jersey). ISBN: 978-0-471-47756-3. 672.

Pletcher D and Walsh F (1990). *Industrial Electrochemistry* 2nd edition (Chapman and Hall Ltd, .ISBN 0412304104. 653.

Pohjoranta A and Tenno R (2007). A Method for Micro via-Fill Process Modeling in a Cu Plating System with Additives. *Journal of Electrochemical Society* **154**(10) D502-D509.

Subramanian VR (2006). Computer facilitated mathematical methods in chemical engineering-similarity solution. *Chemical Engineering Education* **40**(4) 307-312.

Takahashi Ken M and Gross Mihal E (1999). Transport Phenomena *t*hat Control Electroplated Copper Filling of Submicron Vias and Trenches. *Journal of Electrochemical Society* **146**(12) 4499-4503.

Valluri SR, Jeffrey DJ and Corless RM (2000). Some applications of the Lambert W function to physics. *Canadian Journal Physics* **78**(9) 823-831.

Vereecken P, Binstead R, Deligian*n*i H and Andricacos PC (2005). The chemistry of additives in damascene copper plating. *IBM Journal of Research and Development* **49**(1) 3-8

Weisstein Eric W (No Date). Lambert W-Function. *From* Web Resource. Available: http://mathworld.wolfram.com/LambertW-Function.html,http://functions.wolfram.com/ElementaryFunctions/ProductLog/